Estimation of cave geometry using a constrained velocity model inversion with passive seismic data

by R.A. Lynch* and E.C. Lötter*

Synopsis

Careful monitoring of the position of the cave front is essential for well-managed block cave mining. Seismic monitoring systems yield 3-D information about the location of fracturing ahead of the cave. However, because the aseismic gap between cave surface and seismogenic zone is of unknown extent, the cluster of micro-seismicity can only yield an upper bound for the cave height. The large velocity contrast between the fractured rock in the aseismic gap and the broken loose material within the cave can be used by an inversion procedure to find a few simple geometric parameters (such as height of the top of the cave) if a simple 3-D shape—for example a paraboloid—is assumed for the cave. Ray-tracing must be used as the large velocity contrasts cause seismic waves to bend around the cave, but the inversion takes the form of a minimization problem in only a few dimensions and so the computational time is feasible. This technique has been successfully tested on realistic synthetic data.

Introduction

The cost-effective nature of block-cave mining has resulted in an increasing number of such operations worldwide. An essential feature of the mining method is a lack of tight controls over the cave propagation, and thus accurate geotechnical monitoring of the position of the cave surface is important. Tragic accidents such as Northparkes mine in 1999 (Hebbelwhite, 2003) have emphasized this requirement with hindsight. Micro-seismic monitoring has emerged as the most reliable tool for monitoring of cave propagation (Glazer and Hepworth, 2005), and so such monitoring systems have become standard for caving mines around the world. It is thus natural to explore what information is present in the seismic data.

Typically the location of fracturing ahead of the cave is used to infer indirectly the position of the cave. While simple to routinely implement, this approach is unfortunately subject to some error as the seismogenic zone in which the recordable fracturing takes place is some (unknown) distance ahead of the cave surface—see Figure 1. In addition, the events are usually located under a linear-ray assumption, which may not hold in the cave environment depending on event location. Ray-tracing could be used to more accurately locate the seismic events, but this requires an accurate 3-D velocity model, which in turn requires knowledge of the cave geometry—the very information that is being sought from the seismic data.

One standard technique that one could imagine might lead to an estimate of the cave front position is passive seismic tomography. This has been tried in underground (non-caving) mines by many authors, for example see (Young, 1990; Maxwell and Young, 1993; Dubinski, 1997; Maxwell and Young, 1997; Friedel and Williams, 1997; Manthei, 1997; Mutke *et al*., 2001; Lurka, 2005; Debski, 2006). The standard approach is to assume linear seismic ray-paths as this is much computationally faster than the use of ray-tracing. Then the velocities of different spatial cells are treated as adjustable parameters and the minimization cost-function is the total difference between observed and expected seismic wave arrival times for many seismic events and many sensors. Standard minimization techniques accordingly lead to estimates of the 3-D velocity model. The linear-ray assumption is a good one for many underground mines where the maximum velocity differences across the mine are of the order of a few per cent. This kind of passive tomography technique is quite commonly performed in Polish coal mines (see for example Lurka, 2002). However, in the caving environment the velocity difference between intact rock and broken material within the cave can be 80% or more, and so the assumption of linear seismic ray-paths is certainly not valid for events occurring close to the cave (the majority of the mining induced seismicity). Thus the standard passive tomography is of limited use in caving mines.

* *ISS International Limited.*

Estimation of cave geometry using a constrained velocity model inversion

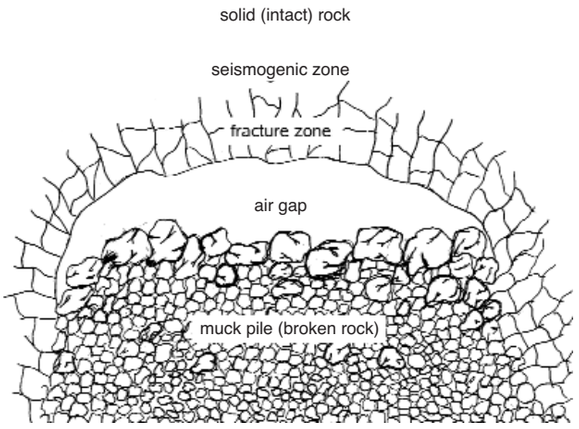

Figure 1—Schematic diagram of the different elements of a cave: the seismogenic zone in which recordable fracturing is taking place, the fractured zone surrounding the cavity, and the cave filled with broken rock (and sometimes an air gap)

This paper explores a different technique in which seismic arrival time data is used to invert for a few geometric parameters of a pseudo-realistic velocity model. The approach is a constrained passive tomography with 3-D ray-tracing.

Procedure

Our technique makes an initial estimate of the cave geometry and uses this to build a simplified 3-dimensional velocity model. This velocity model is then used to perform 3-D ray-tracing and relocate the seismic events. The location residual—the difference between expected and observed seismic wave arrival times- is cumulated for all events and the total location residual used as a cost function to judge how accurate the initial estimate of cave geometry was. Then another estimate for cave geometry is made, the process repeats and so a standard minimization problem is posed. The elements of this procedure are discussed in more detail below.

Velocity model

Some elements of the velocity model of a block-cave mine are known with a degree of accuracy: the material properties (Young's modulus, Poisson's ratio and density) and geometry of the different host rock units (prior to caving) and the approximate footprint of the cave. The only substantial unknowns in our problem are the location of the cave roof and the shape (thickness) of the fracture zone surrounding the cave. If an assumption is made that the cave roof is smoothly and slowly varying in space, then a simple model can be constructed. For example, the cave could be assumed to be parabolic, rising from the known outline on the mining level to a peak somewhere above the mining level. Such a shape has only 3 unknown parameters: the 3-D coordinates of the peak of the cave. If the fracture zone is assumed to be a constant thickness surrounding the cave, then only one additional unknown parameter is added to the problem. We denote the set of parameters specifying the velocity model as **a**.

Then we would have three velocity zones: the caved/broken rock, fracture zone and intact host rock. The intact rock velocities are usually known to about ±5% from calibration blasts carried out prior to caving or in parts of the mine where intact rock is assured. In the fracture zone, P-wave velocities are not expected to change considerably from those of the host rock, while the S-wave velocity would probably be about 10% lower (e.g. see Boadu and Long, 1996). We have used a set of constant velocities for the fracture zone: a future refinement could have smoothly decreasing velocities within the fracture zone as distance to the cave surface decreased.

Within the cave, seismic wave velocities are slowed down considerably by the presence of voids between rock fragments. The details of fragmentation may be unknown and therefore the exact values of the velocities are difficult to estimate. However, these velocities are typically very low—less than 20% of the intact rock. Additionally the attenuation in this zone is very high. Consequently, it is safe to assume that the fastest ray-paths between a fracture outside of the cave and seismic sensors on the opposite side will not be through the broken material within the cave. Thus any low seismic wave velocity can be used within the cave: we have used 500 m/s for v_p in this work.

Ray-tracing

As discussed previously, the large velocity contrasts in the block-cave environment invalidates assumptions of straight seismic ray propagation, and thus ray-tracing is required. The velocity discontinuity across the cave surface from fracture zone to broken rock makes standard shooting or bending techniques numerically unstable. A finite-difference method was implemented and used to pre-compute the travel times between each sensor and every point on a 3-D regular grid. Bilinear extrapolations were used to estimate the travel times to arbitrary seismic event locations based on the travel times to the 8 vertices of the surrounding cell. Tests confirmed this algorithm remains accurate even in the presence of discontinuities.

Minimization

There are two minimizations required in this procedure: a minimization performed in the 'inner' loop when relocating each of the seismic events using ray-tracing with the trial velocity model, and an 'outer' minimization that seeks to find the optimum velocity model. The minimization for straight-ray location of the *j* seismic event is usually just a Simplex method (Press *et al.*, 1989) running on the reduced 3-variable first norm cost function:

$$c_j(\boldsymbol{r}_o) = \sum_i \left| T_{ij}^P - \left\langle T_j^P \right\rangle - \frac{d_{ij}}{v_P} + \frac{\left\langle d_j \right\rangle}{v_P} \right| + \left| T_{ij}^S - \left\langle T_j^S \right\rangle - \frac{d_{ij}}{v_S} + \frac{\left\langle d_j \right\rangle}{v_S} \right| \quad [1]$$

where $\boldsymbol{r}_o$ is the unknown 3-dimensional hypocentre to be found, T_i^P is the observed (picked) arrival time of the P-wave at the *i* sensor, d_i is the straight-ray distance between $\mathbf{r}_o$ and the *i* sensor and $\langle\rangle$ denotes an average over the *i* sensors. For

Estimation of cave geometry using a constrained velocity model inversion

simplicity here a homogeneous velocity model has been assumed. With ray-tracing on an inhomogeneous velocity model parametrized by **a**, the travel time term $v\frac{d_i}{P}$ is explicitly calculated for each sensor location. This adds significantly to the computational time. The modified cost function is now:

$$c_j(\boldsymbol{r}_o,\boldsymbol{a}) = \sum_i \left| T_{ij}^P - \left\langle T_j^P \right\rangle - t_{ij}^P(\boldsymbol{a}) + \left\langle t_j^P(\boldsymbol{a}) \right\rangle \right| + \left| T_{ij}^S - \left\langle T_j^S \right\rangle - t_{ij}^S(\boldsymbol{a}) + \left\langle t_j^S(\boldsymbol{a}) \right\rangle \right| \quad [2]$$

The minimization space, however, now becomes more convoluted, and often the Simplex method settles in local minima. This necessitates many restarts of the Simplex algorithm, or even combination of Simplex with other methods: the Genetic and Simulated Annealing methods have been useful in this regard. Minimization of this function with respect to $\mathbf{r}_o$ leads to the event (re)location.

The minimum value of the cost function, $c_j(\mathbf{a})$, for the j seismic event is then summed to provide a grand cost function for the outer minimization, dependant on the parameters of the velocity model **a**:

$$C(\boldsymbol{a}) = \sum_j c_j(\boldsymbol{a}) \quad [3]$$

The grand cost function $C(\mathbf{a})$ is minimized using a hybrid Simplex/Genetic scheme to find values of the velocity model parameters **a** that result in the lowest average mismatch between expected and observed seismic wave arrival times. The height and shape of the cave would be contained in the set **a**.

Tests with synthetic data

To test a velocity model on synthetic data, we first have to create synthetic data sets for typical velocity models we would want to invert for. Such data sets will consist of the sensor locations (Δ_1, Δ_2,..., Δ_n), and a table of P- and S-wave arrival times triggered by n seismic events in the seismogenic zone of the region we are inverting.

Construction of synthetic data

To generate synthetic data, we pick a velocity function for the P-waves as a function of position, $v = v\,(x,y,z)$. A rectangular axis-aligned grid of P-wave slowness s_{ijk}^P is initialized to have slowness $s_{ijk}^P = \frac{1}{v(x,y,z)}$ where $x = x_{min} + \frac{i}{I}$, $(x_{max}\text{-}x_{min})$, $y = y_{min} + \frac{j}{J}(y_{max}\text{-}y_{min})$ and $z = z_{min} + \frac{k}{K}(z_{max}\text{-}z_{min})$ at the regular points inside the domain $(x_{min}, x_{max})\times(y_{min},y_{max})\times(z_{min},z_{max})$, with $0 \le i \le I$, $0 \le j \le J$, and $0 \le k < K$,.

We assume that the function $v_{true} = v_a\,(x,y,z)$ represents the true underlying velocity model of the domain, where the vector **a** represents certain unknown parameters which we wish to estimate. When constructing a synthetic data set, we will dictate the value of a as either explicitly dictating the velocities in the model, or implying a certain shape or gradient for inhomogenities in the model.

The (unknown) true event locations $\xi_1,\xi_2,...,\xi_n$ are either uniformly randomly distributed in the domain, or according to a statistical distribution, which will match the seismogenic zone implied by the inhomogenities in the model (which in turn are a function of the parameter **a**). For example, when we are inverting for a homogenous velocity model, the uniform distribution will be sufficient, but when we are considering a cave, the seismogenic zone will exclude the region inside the cave.

Given the true velocity model in the form of the P-wave slowness grid s_{ijk}^P and the true event locations $\xi_1,\xi_2,...,\xi_n$ and their origin times, synthetic P- and S-arrival times can be generated by explicit finite-difference ray-tracing from each of the sensor sites Δ_i to construct a grid G_i^P of synthetic P-arrival times corresponding to sensor site Δ_i, for each $1 \le \mathbf{i} \le \mathrm{m}$. Trilinear interpolation between the grid points of each grid G_i^P yields P-wave travel times t_{ij}^P for the P-wave departing from event ξ_j arriving at sensor Δ_i. A similar procedure is followed for the S-wave travel times. Adding each event's origin time to the obtained travel times (for both the P- and S-waves) results in the synthetic arrival time data $T_{ij}^P = t_{ij}^P + t_j^0$ and $T_{ij}^S = t_{ij}^S + t_j^0$ for each i and j. Random Gaussian noise with $\sigma = 0.0025$s is added to these arrival times, to take into account the possibility of errors in the P- and S-wave arrival picking.

We now consider the arrival time data T_{ij}^P and T_{ij}^S (and the sensor locations Δ_i) as the only observable input to our inversion algorithm. The true underlying velocity model and event locations are therefore assumed to be unknown, and we will utilize only them after inversion to quantify the errors of our estimates.

Inversion of synthetic data

Using the synthetic input data in the form of the 2 mn arrival times T_{ij}^P and T_{ij}^S and m sensor locations Δ_m, an initial estimate of the locations and origin times of the n events can be inverted for using the classical location with the straight ray assumption, to obtain a set of relocated events η_1, $\eta_2,...,\eta_n$. Using some initial estimate for the velocity model parameter **a**, minimization of the cost function [3] is achieved by the alternating perturbation of **a** and relocation of the events η_j as described in earlier.

We consider three synthetic examples, in order of ascending complexity:

Homogenous velocity model

This simple case is done as a 'sanity' test for our algorithm. With the one-dimensional parametrization $\mathbf{a} = (V^P)$ and the one-dimensional parametrized velocity model given by v_a (x, y, z) $= a_1 = v^P$, we considered 100 randomly distributed event locations in the region $[0,1000]^3$, together with 10 randomly placed sensor locations. For the travel time grid, we use equally spaced grid points 40 m apart. We assume that each seismic event triggers all 10 sensors, and thus a set of 100 x 10 = 1000 synthetic P-wave arrival times are constructed on the grid T_{ij}^P, with random noise ($\sigma = 0.0025$s)) added, where we use the velocity model $v_{true} = v_{(5000.0)}$ $(x,y,z) = 5000.0$ as a representation of the true underlying velocity model with a constant P-wave velocity of 5000 m/s and $v_S = \frac{VP}{1.65}$.

The resulting P- and S-wave travel times are used as input for the inversion procedure. First, using the straight ray assumption (which incidentally is valid for this model), we estimate the initial seismic event locations η_1, $\eta_2,...,\eta_n$, using the parametrized velocity model $v_{(3000.0)}$ (x,y,z), as a naive initial guess of P-wave velocity in the region of interest.

Estimation of cave geometry using a constrained velocity model inversion

Subsequent minimization of the cost function results in the initial parameter **a** = (3000.0) converging to **a** = (5097.96). Comparing the relocated events with the true event locations, we find the average error $|\eta_i - \xi_i|$ to be 49.064 m, and the average mislocation error as a percentage of average hypocentral distance as 7.298 %. Repeating the inversion with progressively finer grid spacings leads to the results in Table I, which summarizes three runs of the minimization procedure using different grid spacings. In each case an initial constant P-wave velocity of 3000 m/s is used. The last column expresses the average mislocation as a percentage of average hypocentral distance.

It is clear that although the running time for coarser grids is significantly lower, greater accuracy is achieved by opting for finer grid spacing.

The histograms in Figures 2 and 3 respectively give the distribution of time residua at the start of the minimization procedure (**a** = (3000.0)) against the distribution at the end of the minimization, showing a significant decrease in variance of the errors.

Parabolic cave velocity model

We now consider a synthetic model with a pseudo-realistic cave shape in the form of two parabolic surfaces separating the inner low-velocity zone, the intermediate zone of fractured rock, and the outer zone of undamaged rock. The model will have a two-dimensional parametrization given by **a** = (h, w), where h is the height from the base of the cave to the start of the zone of fractured rock, and w will simultaneously parametrize the vertical and horizontal width of the zone of fractured rock. If we assume the known base of the cave to have a circular shape centred at the point **c** = (c_x, e_y, e_z) and having a radius (in the xy plane) of r, the inner and outer surfaces can respectively be expressed as having boundaries defined by the sets of formulae

$$z = c_z - h\left(1 - \frac{\left(c_x - x^2\right) + \left(c_y - y^2\right)}{r^2}\right); z = c_z \qquad [4]$$

and

$$z = c_z - h - w\left(-\frac{\left(c_x - x^2\right) + \left(c_y - y^2\right)}{\left(r + w\right)^2}\right)$$
$$(h + 2w); z = c_z + w. \qquad [5]$$

We use these boundary values to define which P- and S-wave velocities should be assigned to each grid point, depending on which zone they fall in, as shown in Table II. The P-wave velocities observed in the intermediate and outer zones are identical, as discussed earlier, while the intermediate zone S-wave velocity is 10% less than that of the intact zone.

Table I

Running times on a 32 bit P.C. with 2.0 GHz CPU

Run	Grid	Time	Converged a	Avg.mislocation	Error
1	40 m	1:06	(5097.96)	49.064	7.30%
2	20 m	5:34	(5012.87)	19.476	3.00%
3	10 m	47:45	(5006.13)	16.367	2.43%

It is clear that the combination of this information describes two parametrized velocity models of the two variables h and w of the form $v_a^W(x, y, z) = v_{(h,w)}^W(x,y,z)$, where the superscript W refers to either the P-wave or the S-wave. Assuming that the true underlying velocity model (cave) has its footprint centred at the point c = (5000.0, 500.0, 700.0) with a radius of r = 300.0 (known parameters before inversion), and has a true height of h = 500.0 and fractured zone width of w = 100.0 (unknown parameters before inversion), a minimization problem similar to the previous example is posed. The only essential extension is that ray tracing is now done separately on the grid of P-wave slownesses and S-wave slownesses.

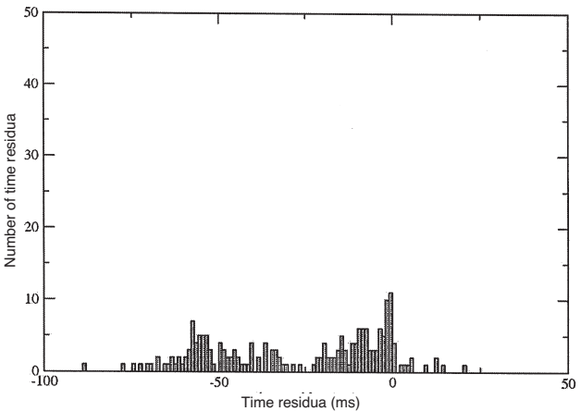

Figure 2—Histogram of time residua before inversion with standard deviation of σ = 6.963 ms

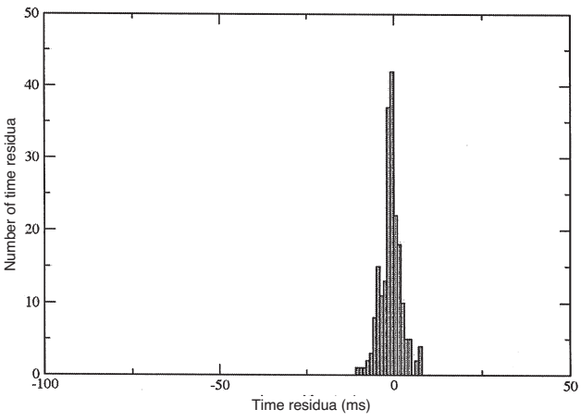

Figure 3—Histogram of time residua after inversion- now σ = 0.154 ms, much closer to 0.0 as expected

Table II

P and S-wave velocities for the isotropic inhomogeneous medium

Zone	Pressure wave	Shear wave
Inner (cave)	500 m/s	300 m/s
Intermediate (seismogenic zone)	5500 m/s	3150 m/s
Outer (intact rock)	5500 m/s	3500 m/s

Estimation of cave geometry using a constrained velocity model inversion

Choosing an initial value of the parameter **a** as **a** = (h,w) = (300.0, 50.0), Table III summarizes the results for respective grid spacings of 10 m, 20 m and 40 m.

The histograms of Figures 4 and 5 give the distribution of arrival time errors at the start of the minimization procedure (with **a** = (300.0, 50.0)) against the distribution at the end of the minimization, showing the significant decrease in variance of the errors.

Merged parabolic caves velocity model

As a natural extension to the parabolic velocity model considered, we now consider a merged model of two, copies of the parabolic cave model considered earlier. Consequently, we label the known parameters of the two parabolic caves as $\mathbf{c}_1$, $\mathbf{r}_1$ and $\mathbf{c}_2$, $\mathbf{r}_2$ respectively, where for the joint velocity model we assume that the z-component of $\mathbf{c}_1$ and $\mathbf{c}_2$ are equal (corresponding to the fact that both caves have known bases of equal depth). On the other hand, the two cave models have unknown dimensions characterized by the parametrizations (h_1, w_1) and (h_2, w_2), in each case corresponding to the inner cave height and fractured zone width. For the merged velocity model we assume that w_1 = w_2, and therefore obtain the 3D parametrization (h_1, h_2, w).To prescribe P- and S-velocities to points in the merged parabolic caves velocity model, we classify an arbitrary point in the velocity model to be

- in the inner (cave) zone if the point is in either the inner (cave) zone of one of the constituent single parabolic cave models
- in the intermediate (seismogenic) zone if it is not in the inner zone and in the intermediate zone of one of the constituent single parabolic cave models and
- in the outer (intact) zone otherwise.

After the classification of an arbitrary point in the new model into one of the three zones, the same P- and S-velocities are prescribed as in Table II.

After generating synthetic data with the assumption that the two caves have respective heights of h_1 = 300, h_2 = 200 and share a seismogenic zone width of w = 100, based on the known parameters $\mathbf{c}_1$ = (400,400, 700), r_1 = (200) and $\mathbf{c}_2$ = (600, 500, 700), $\mathbf{r}_2$ = (150), we perform various inversions of the data using an initial value of (h_1, h_2, w) = (100, 100, 50). The resulting running times and inversion results are given in Table IV.

Table III

Running times on a 32– bit PC with 2.0 Ghz CPU and convergence for synthetic data inversion of the parabolic model with independent P and S wave velocity structure. The true value of a is (500,100)

Run	Grid	Time	Converged a	Avg. mislocation	Error
1	40m	8:14	(486.29,104.74)	28.56	5.30%
2	20m	41:08	(497.97,101.75)	15.45	2.78%
3	10m	5:47:36	(498.30,104.95)	14.22	2.62%

Observations and conclusions

The large velocity contrasts present in caving environments rule out the use of standard linear-ray passive tomography inversions in order to estimate reliably the velocity model and therefore the cave front position. Using 3-D finite-difference ray-tracing with a standard tomography scheme, in which many free parameters (the velocity of each cell) are inverted for, is not practical with the current PC processor speeds. Our

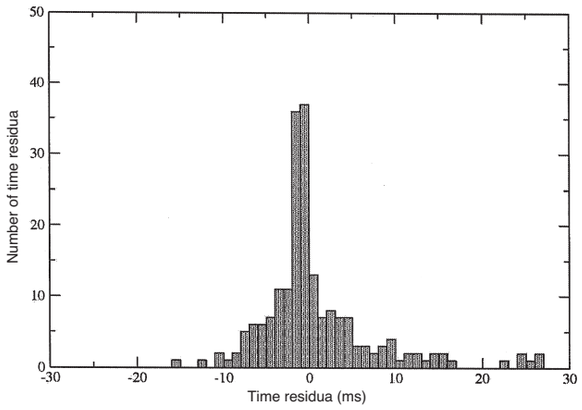

Figure 4—Histogram of time residua before inversion, σ = 4.851 ms

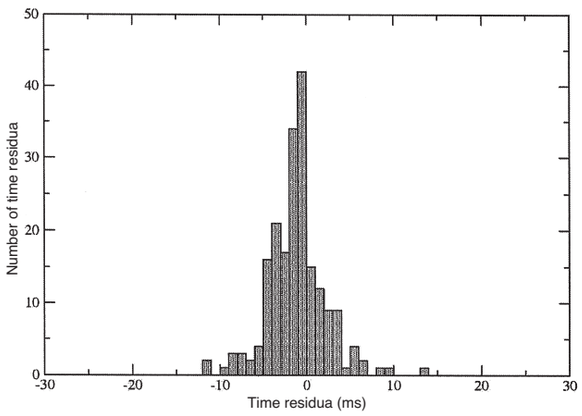

Figure 5—Histogram of residua after inversion, σ = 2.378 ms

Table IV

Running times on a 32– bit PC with 2.0 GHz CPU and convergence for synthetic data inversion of the merged parabolic model with independent P and S wave velocity structure. The true value of a is (300,200,100)

Run	Grid	Time	Converged a	Avg. mislocation	Error
1	40 m	17:57	(336.50,227.83,74.82)	26.90	5.60%
2	20 m	1:07:55	(311.04,182.68,93.42)	14.06	2.93%
3	12.5 m	4:05:52	(312.89,215.54,97.99)	12.85	2.64%

approach significantly reduces the number of inversion parameters by making some realistic geometric simplifications—for example that the cave shape can be well modelled by a few parabolic surfaces. The known information, for example the cave footprint, is added explicitly to the problem, and the resulting inversion has proved to be both tractable and stable for the experiments with simulated seismic data.

Three test cases were reported here. In the simplest case—a homogeneous velocity model—only 1 parameter, v_p, was inverted for. This trivial case was useful as a 'sanity' check for our algorithm. The more realistic cases—one and two parabolic surfaces—approached the real situation of a block cave mine. In these cases, computer time of 4–6 hours was used to find the 'true' geometric parameters to within 5%–7%, with events being relocated to within a few per cent of average hypocentral distance from the 'true' locations.

These results are encouraging. It would appear that it is feasible to estimate the position of the cave front and thickness of the fracture zone from passive seismic data using this technique. Furthermore, the more accurate seismic event locations would aid the standard methods of cave front estimation being routinely applied now.

References

Boadu, F.K. and Long, L.T. Effects of fractures on seismic-wave velocity and attenuation, *Geophysical Journal International*, vol. 127, pp. 86–110.

Debski, W. Tomography imaging through the Monte Carlo sampling, *PUBLS. INST. GEOPHYS. POL. ACAD. SC.*, M-29, 1996. 2006. p. 395.

Dubinski, J. Assessment of rock burst prevention using seismic profiling and tomography techniques in Polish coal mines, *4th International Symposium on Rockbursts and Seismicity in Mines*, S. Gibowicz and S. Lasocki (eds.), Balkema. 1997.

Friedel, D., Scott, M.J., and Williams, T. Temporal imaging of mine-induced stress change using seismic tomography, *Engineering Geology*, vol. 46, no. 2, 1997. pp. 131–141.

Glazer, S. and Hepworth, N. Seismicity induced by cave mining, Palabora experience, *6th International Symposium on Rockbursts and Seismicity in Mines*, Y. Potvin and M. Hudyma (eds.), Australian Centre for Geomechnics. 2005.

Hebblewhite, H. Northparkes findings—the implications for geotechnical professionals in the mining industry, *The First Australasian Ground Control in Mining Conference*. 2003.

Lurka, A. Seismic hazard assessment in the Bielszowice coal mine using the passive tomography, *Seismogenic Process Monitoring*, H. Ogasawara, Y. Yanagidani, and M. Ando (eds.), Balkema. 2002.

Lurka, A. Location of mining induced seismicity in zones of high p-wave velocity and in zones of high p-wave velocity gradient in Polish mines, *6th International Symposium on Rockbursts and Seismicity in Mines*, Y. Potvin and M. Hudyma (eds.), Australian Centre for Geomechanics. 2005.

Manthei, G. Seismic tomography on a pillar in a potash mine, *4th International Symposium on Rockbursts and Seismicity in Mines*, S. Gibowicz and S. Lasocki (eds.), Balkema. 1997.

Maxwell, S. and Young, R. A comparison between controlled source and passive source seismic velocity images, *Bulletin of the Seismological Society of America*, vol. 83, no. 63, 1993. pp. 1813–1834.

Maxwell, S.C. and Young, R.P. Seismic velocity inversion from micro seismic data, *Seismic Monitoring in Mines*, A.J. Mendecki (ed.), Chap. 6, Chapman and Hall, London. 1997. pp. 108–118.

Mutke, G., Lurka, A., Mirek, A., Bargiel, K., and Wrobel, J. Temporal changes in seismicity and passive tomography images: a case study of Rudna copper ore mine—Poland, *5th. International Symposium on Rockbursts and Seismicity in Mines*, G. van Aswegen, R. Durrheim, and W. Ortlepp (eds.), South African Institute of Mining and Metallurgy. 2001.

Press, W.H., Flannery, B.P., Teukolsky, S.A., and Vetterling, W.T. *Numerical Recipes: The Art of Scientific Computing*, Cambridge University Press. 1989.

Young, R. Geotomography in the study of rockbursts and seismicity in mines, *2nd International Symposium on Rock bursts and Seismicity in Mines*—Minnesota, C. Fairhurst (ed.), Balkema. 1990. ◆